OPEN

PRS GLOBAL OPEN EXPERIMENTAL

Quantification of Collagen Organization after Nerve Repair

Jacqueline S. Israel, MD*
Corinne R. Esquibel, PhD†
Aaron M. Dingle, PhD*
Yuming Liu, PhD†
Adib Keikhosravi, MS†‡
Jane A. Pisaniello, BS‡
Madison A. Hesse*
Sarah K. Brodnick, BS‡
Joseph Novello, MS‡
Lisa Krugner-Higby, DVM, PhD§
Justin C. Williams, PhD‡
Kevin W. Eliceiri, PhD†‡
Samuel O. Poore, MD, PhD*‡

Background: Clinical outcomes after nerve injury and repair remain suboptimal. Patients may be plagued by poor functional recovery and painful neuroma at the repair site, characterized by disorganized collagen and sprouting axons. Collagen deposition during wound healing can be intrinsically imaged using second harmonic generation (SHG) microscopy. The purpose of this study was to develop a protocol for SHG imaging of nerves and to assess whether collagen alignment can be quantified after nerve repair.

Methods: Sciatic nerve transection and epineural repair was performed in male rats. The contralateral nerves were used as intra-animal controls. Ten-millimeter nerve segments were harvested and fixed onto slides. SHG images were collected using a 20× objective on a multiphoton microscope. Collagen fiber alignment was calculated using CurveAlign software. Alignment was calculated on a scale from 0 to 1, where 1 represents perfect alignment. Statistical analysis was performed using a linear mixed-effects model.

Results: Eight male rats underwent right sciatic nerve repair using 9-0 Nylon suture. There were gross variations in collagen fiber organization in the repaired nerves compared with the controls. Quantitatively, collagen fibers were more aligned in the control nerves (mean alignment 0.754, SE 0.055) than in the repairs (mean alignment 0.413, SE 0.047; $P < 0.001$).

Conclusions: SHG microscopy can be used to quantitate collagen after nerve repair via fiber alignment. Given that the development of neuroma likely reflects aberrant wound healing, ex vivo and/or in vivo SHG imaging may be useful for further investigation of the variables predisposing to neuroma. *(Plast Reconstr Surg Glob Open 2017;5:e1586; doi: 10.1097/GOX.0000000000001586; Published online 11 December 2017.)*

INTRODUCTION

Despite remarkable experimental advances in the processes underlying nerve regeneration, functional outcomes after nerve injury and primary epineural repair remain unpredictable.[1,2] Individuals may experience functional deficits, and painful neuroma, characterized by a focal collection of disorganized collagen and aberrant sprouting axons. Major obstacles to improving clinical outcomes is a general lack of understanding of the optimal ways by which to consistently ensure end-organ reinnervation in a timely fashion and prevent neuroma.[3]

Collagen production and remodeling are key stages in wound healing that occur in the majority of living tissues, beginning with fibroblast and myofibroblast proliferation at approximately 3–4 days after injury, and continuing with collagen reorganization and maturation for up to 1 year.[4] Nerve healing is no exception. Type I, III, IV, and V collagen are all present in the peripheral nervous system, with types I and III predominating during wound healing after injury.[5] A plethora of intrinsic and extrinsic factors dictate whether wound healing occurs optimally or in an aberrant fashion, with excessive fibrosis or inadequate cross-linking being examples of collagen maturation gone awry.[6]

*From the *Division of Plastic Surgery, Department of Surgery, University of Wisconsin – Madison, Wis.; †Laboratory for Optical and Computational Instrumentation, University of Wisconsin – Madison, Wis.; ‡Department of Biomedical Engineering, College of Engineering, University of Wisconsin – Madison, Wis.; and §Department of Surgical Sciences, School of Veterinary Medicine, University of Wisconsin – Madison, Wis.*

Received for publication August 29, 2017; accepted October 13, 2017.

Presented in electronic poster format at the American Society of Peripheral Nerve Annual Meeting, January 2017, Waikoloa, Hawaii.

DOI: 10.1097/GOX.0000000000001586

Disclosure: *The authors have no financial interest to declare in relation to the content of this article. The Article Processing Charge was paid for by the authors.*

Differences in collagen during wound healing can be intrinsically imaged via second harmonic generation (SHG) on a multiphoton laser-scanning microscope.[7] SHG is a nonlinear, coherent optical process during which two photons combine, emitting single photon with visible light.[7–10] With the use of a laser-scanning microscope,[11] SHG allows for three-dimensional imaging of non-centrosymmetric structures (eg, those that do not have a "center of symmetry"[8]),[9] with a depth penetration of up to 500 μm.[12,13] The triple-helix structure of fibrillar collagen permits visualization with SHG microscopy.[5,8,10,14,15] This technology results in little to no tissue damage and does not require the use of fluorescent labels, stains, or genetically modified species.[7,10,16,17] The purpose of this study was to develop and test a protocol for imaging repaired nerves using SHG, and quantitatively compare collagen alignment in repairs to controls.

METHODS

Nerve Repair

The Institutional Animal Care and Use Committee (IACUC) approved all animal procedures. We performed transection and repair of the right sciatic nerve in male Sprague Dawley rats weighing approximately 280 g. General anesthesia was achieved using isoflurane anesthetic via nasal cone (3–5% induction, 1.5–2% maintenance). Pain was controlled using subcutaneous injections of buprenorphine (0.05 mg/kg, concentration 0.03 mg/mL). The adequacy of anesthesia was assessed by toe pinch and the right hind limb was shaved and prepped. The sciatic nerve was exposed using a posterolateral approach, and the nerve was identified as it emerged from the sciatic notch and trifurcated into the tibial, peroneal, and sural nerves. Transection of the nerve was performed using microsurgical scissors, 33 mm proximal to the location of the greatest diameter of the gastrocnemius muscle. Epineural neurorrhaphy was performed using 9-0 Nylon suture (Ethicon Inc., Somerville, N.J.) and a Zeiss operating microscope. The minimum amount of suture that facilitated coaptation of the epineurium with little to no outpouching of the fascicles was used. The biceps femoris muscle was reapproximated using a running 4-0 Vicryl suture (Ethicon Inc, Somerville, N.J.) and the skin was closed in two layers with buried 4-0 Vicryl sutures and staples. The animals were recovered from anesthesia and staples were removed 2 weeks postoperatively.

After euthanasia at approximately 4 weeks postoperatively, 10-mm segments of repaired nerve were harvested. The uninjured sciatic nerve of the contralateral limb served as an intra-animal control. Before fixation, specimens were pinned at native resting tension to prevent recoil. The specimens were fixed in 4% paraformaldehyde overnight at 4°C, processed in graded alcohol solutions, and passively mounted onto glass slides under no strain. The decision to mount the specimens passively is supported by previous work by Vijayaraghavan et al.,[7] which suggests that when imaging injured nerves, placing zero strain on the samples avoids alterations in tissue morphology.

Image Acquisition

Ex vivo SHG images in the backward direction were collected through a Zeiss 20× water-dipping objective (1.0 NA) at 890 nm excitation. A dichroic cube filter set (Chroma Technologies, Bellow Falls, Vt.) containing two band-pass emission filters—one for SHG (445/40 bandpass) and one for FAD (592/100 bandpass) was utilized. The upright multiphoton imaging system consisted of a multialkali photomultiplier detector (Hamamatsu, Shizuoka, Japan) on a Bruker Ultima IV (Bruker FM, Middleton, Wis.) multiphoton microscope equipped with an Insight ultrafast laser (Spectra Physics, Santa Clara, Calif.). A motorized stage was used to automatically collect three-dimensional images that were collected at tiled x–y locations throughout the nerve sections. Individual images from each x–y location were stitched together into fused montage images using a FIJI plugin. Maximum intensity projections were used to display three-dimensional resolution in a single plane. A 1- × 1-mm area of interest was identified on each fused image. Three representative optical slices (in the z axis) were selected from each fused image for quantitative analysis.

Histology

After fixation and imaging, qualitative histological assessment of the nerve was performed. Tissue sections (5 μm thick) were stained with Hematoxylin and Eosin (H&E), Gömöri's Trichrome (GTC), and picrosirius red (PSR). An upright Nikon Eclipse E600 microscope equipped with a Nikon polarizing filter (Nikon, Tokyo, Japan) and CELLSENS acquisition software (Olympus, Tokyo, Japan) were used to take representative photomicrographs of serial sections. The three most superficially sectioned slide images were then correlated with the SHG images to facilitate qualitative comparison between images. The comparison images were collected using CAMM image acquisition: After generating a circularly polarized laser beam, it was focused on the sample using a 40×/1.25-NA water immersion objective (Nikon, Melville, N.Y.). The second harmonic signal was separated using a 390/18-nm filter (ThorLabs, Newton, N.J.).

Analysis

CurveAlign, our open-source software platform, was used to quantify the collagen fiber alignment in each area of interest.[18–20] Individual fibers were extracted by CT-FIRE mode using default parameters. The overall alignment of the extracted collagen fibers was calculated using the circular statistics toolbox incorporated in the platform.[21] Alignment represents the similarity of fiber orientations, ranging from 0 to 1, where 1 indicates that all fibers are oriented in the same direction. A linear mixed-effects model with random intercepts was used to account for within-sample variability.[22] A P-value of <0.05 was deemed statistically significant.

RESULTS

Eight male Sprague Dawley rats underwent right sciatic nerve transection and epineural repair. There were no

anesthesia-related or intraoperative complications. The animals were euthanized at a mean of 28 days postoperatively (standard deviation 5 days). Qualitatively, SHG microscopy revealed gross variations in collagen fiber organization in repaired nerves compared with uninjured controls (Figs. 1, 2). Collagen fibers (green) were selectively visualized via the SHG 445/40 bandpass filter at 890 nm. Synthetic suture material (Fig. 1), perineural vasculature and red blood cells, skeletal muscle fibers, and hair are all visualized via autofluorescence (in red). Figure 2 depicts examples of repair and control nerve specimens imaged using the SHG technique.

Quantitative assessments were possible using CurveAlign software and calculation of fiber alignment, and are not apparent with visual inspection alone. Analysis of collagen fiber alignment revealed quantitative trends that were consistent with the qualitative differences described above. The collagen fibers were more aligned in the control samples (mean alignment 0.754, standard error 0.055) than in the repair samples (mean alignment 0.413, standard error 0.047; $P < 0.001$).

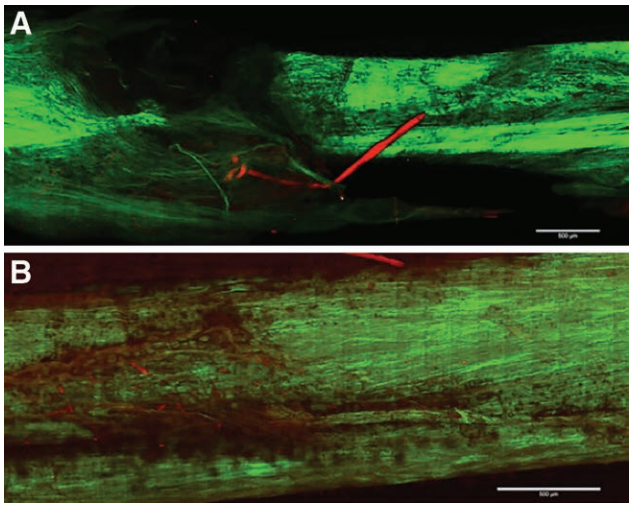

Fig. 1. Maximum intensity projection SHG images of nerve samples (fibrillar collagen = green, autofluorescence = red). A, Repaired nerve #1, epineural repair, 4 weeks after repair. The Nylon suture material is visible in red. B, Control #1, uninjured sciatic nerve from left hind limb. Scale bar 500 µm.

There were similarities in the overall gross morphology and qualitative appearance of the longitudinal histologic sections compared with the SHG images (Fig. 3). SHG facilitated high-resolution, three-dimensional, intrinsic imaging of collagen fibers. Example SHG images are depicted adjacent to sectioned nerve samples stained with traditional histological preparations including H&E, GTC, and PSR in Figure 3. SHG allows for acquisition of an image that appears qualitatively similar to those using traditional stains but, importantly, does not require the same staining and processing as other methods. In comparison with commonly used histological stains to assess collagen (such as picrosirius red), SHG microscopy is not biased by fluorescence or staining based changes as no fluorescence or staining is needed (Fig. 3).

DISCUSSION

Peripheral nerve injury is common, affecting up to 5% of all trauma patients.[23,24] Traumatic nerve injury is associated with paralysis, weakness, numbness, chronic pain, and other issues that significantly impair productivity and quality of life.[24,25] Despite refined microsurgical techniques and a growing body of neurobiological literature, functional outcomes (especially motor function) after nerve repair remain unpredictable.[1–3,26–29] The processes *reinnervation* and *regeneration* are both essential for restoration of function after nerve repair, and the persistence of suboptimal clinical outcomes supports ongoing neurobiological investigation of the wound healing processes underlying nerve regeneration.[30]

Collagen production after nerve injury is mediated primarily by transforming growth factor beta but also may be affected by a multitude of intrinsic and extrinsic cell signaling pathways and molecular interactions in the local regenerative milieu.[5,31] According to Dahlin et al.,[31] "the intrinsic growth capacity of peripheral nerve regeneration has to be combined with a proper environment to encourage axonal growth," and this growth capacity may be hindered by excessive production and/or improper reorganization of collagen, preventing appropriate axonal sprouting and leading to neuroma.[5] Surgical repair may exacerbate collagen production due to the presence of foreign body (sutures), unintentional tension at the repair site, and further

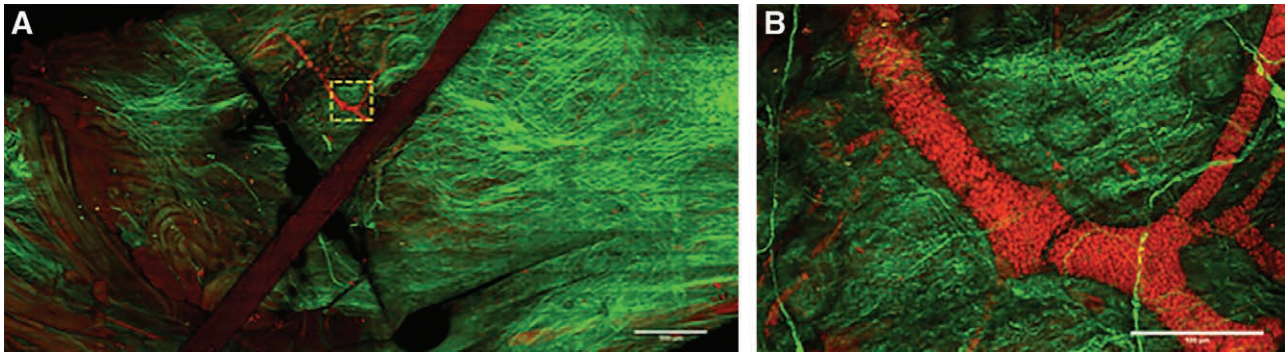

Fig. 2. SHG images of repair and control nerve samples. A, Repaired nerve #2, epineural repair, 4 weeks after repair. Box inset is enlarged and depicted on the right. Scale bar 500 µm. B, Enlarged inset from repaired nerve. Perineural vasculature (with intravascular biconcave red blood cells) is depicted in red (autofluorescence). Scale bar 100 µm.

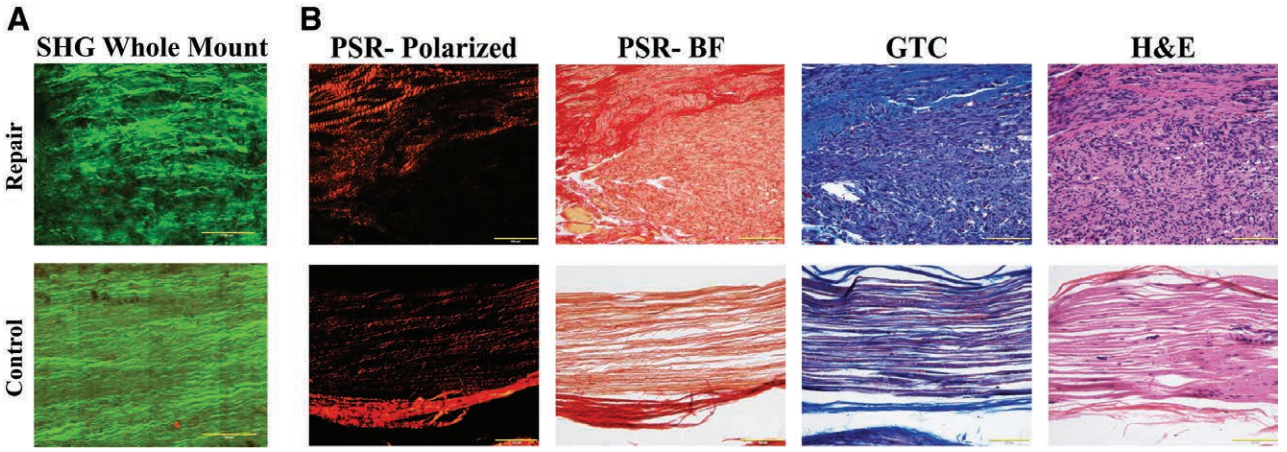

Fig. 3. Qualitative comparison of nerve specimens imaged using SHG microscopy (far left) and traditional histologic preparations. The same nerve specimen is imaged using a variety of methodologies, depicted as examples here. A, SHG three-dimensional images of nerve specimens before histological processing. The collagen fibers are imaged intrinsically without sectioning or the application of stains or dyes for imaging. B, Appearance of the same nerve posthistological processing (fixation, embedding, sectioning, staining) using PSR, GTC, and H&E stains. Although each technique allows for qualitative visualization of collagen at the repair site, collagen is depicted in different colors, depending on the stain. The gross morphology of each of the images is the same though each imaging/processing technique allows for visualization of nuances in the tissue and cellular structures being imaged. Scale bar for all images 100 μm.

vascular insult via nerve dissection.[5] We sought to selectively image and subsequently quantify collagen at the repair site of repaired nerves using SHG microscopy.

To our knowledge, SHG has not previously been used to study nerve repair after transection. Previous studies involving SHG and peripheral nerves have focused on testing ideal imaging parameters and variables affecting image quality, such as inherent viscoelastic properties and specimen preparation.[7,12] We found that by visual inspection the collagen at and around the repair site in the injured nerve group appeared randomly organized with the presence of fractured and/or wavier individual fibers and more scattered groups of fibers. This was in contrast to the control nerves, in which the individual fibers appeared linear and arranged in parallel groups of fibers. These findings are similar to previous studies, such as Bueno et al.,[8] who found that the control tissue (healthy human cornea) revealed a much more "regular" arrangement of collagen compared with pathologic specimens (human cornea with keratoconus) in which the collagen morphology was random and disorganized.

SHG microscopy provides selective qualitative and quantitative information about collagen and offers distinct benefits over histologic techniques, immunohistochemistry, and fluorescence microscopy.[14] Quantitative analysis in this study was possible by calculating fiber alignment. Histologic stains, including GTC (in which collagen appears either green or blue) and PSR, also facilitate visualization of collagen but are associated with some limitations. First, in our specimens we observed significant fracturing of the nerves when sectioning longitudinally. This diminished the specimen quality and limited our histological assessment of collagen. Second, neither GTC nor PSR stains provide the same degree of resolution that can be visualized with SHG, as the latter allows for assessment of individual collagen fibers.[15] PSR staining enhances the natural birefringence of collagen bundles. When viewed under linear polarized light, collagens are revealed as red, orange, yellow, or green fibers. Unfortunately, sample orientation under linear polarized light affects PSR hue and signal strength.[32] SHG microscopy is not subject to this sample orientation issue. Finally, neither histology nor immunohistochemistry can be used to assess tissue in vivo or in situ, and for clinical applicability requires tissue biopsy and subsequent processing. SHG does not require staining or application of an antibody or fluorescent label, and can be used in vivo.[33,34] With further development of deep imaging approaches like adaptive optics,[35] different SHG instrument form factors,[36,37] and SHG endoscopy,[38] there is potential for eventual transition to clinical application.[7]

Since its initial discovery in the second half of the 20th century, SHG has been used to image collagen in a variety of disease processes. Because collagen is the most abundant protein in the human body, SHG microscopy has particular relevance to plastic surgery, and it has been used to study areas such as wound healing and trauma,[16] burns,[14] connective tissue disorders,[39] skin and soft tissue disorders including aging and hemifacial atrophy,[40] fibrotic disorders, skin cancer,[41] breast cancer,[42,43] ovarian cancer,[44] pancreatic cancer,[45] and other malignancies.[7,8,14,17,46] In a study assessing the use of SHG for imaging skin, tendon, endometrium, and liver tissue samples from a variety of species, Cox et al.[15] assert that although it was once a "highly specialized" technique for primary experimental use, SHG microscopy is widely applicable to a variety of biological processes and medical conditions. In a 2006 study of basal cell carcinoma excision using multiphoton fluorescence (MF) and SHG, Lin et al.[41] found that a "MF to SHG index" allowed for differentiation between normal and malignant tissue, suggesting that this technology may one day be employed as an alternative to Mohs excision. Due to current limitations in depth penetration, at present this technology could not be used to assess large peripheral nerves in vivo. Potentially more feasible applications, at present, are

the use of SHG to assess surgical and/or dermatopathology specimens (such as in excised neuroma or skin cancer).

SHG microscopy has potential for future use in diagnosing and managing peripheral nerve injuries. One advantage of SHG microscopy is the optical sectioning ability, which helps image a certain layer at any depth within the nerve (up to 500 µm as mentioned above) without the need for physical sectioning.[13] In nerves, multiphoton microscopy allows for imaging beyond the epineurium, so that the perinerium surrounding the fascicles may also be imaged.[12,13] This will be particularly relevant if multiphoton microscopy can be technically modified to facilitate imaging of greater depths.

A limitation of both the imaging and the histology is the potential change in tension of the nerve after harvest. The cylindrical shape and elastic nature of peripheral nerves present challenges when performing advanced microscopy.[7,47] The nerve is not perfectly flat, and a greater depth of field is required to create a three-dimensional image of the entire width of the nerve; consequently the greater the depth for SHG, the lower the quality of the image.[8] Collagen fibers may have a different appearance when imaged in situ (eg, the nerve is exposed and imaged before resection).[7,12] In situ imaging is a direction for ongoing evaluation. In addition, future application of third harmonic generation microscopy (which allows for imaging of myelin) may facilitate label-free imaging of nerves.[48] Finally, we have focused on collagen fiber alignment as a tool for quantitatively comparing collagen (via fiber alignment) at a specific time point (eg, 4 weeks) after repair. We recognize that different snapshots in time, reflecting different stages of wound healing, and, for example, collagen maturation, may reveal additional nuances in alignment and overall collagen appearance. Future studies may incorporate additional time points, in situ imaging, and analysis of alignment, density, and organization when evaluating the collagen response to nerve injury and comparing various types of nerve repair.[49]

CONCLUSIONS

SHG microscopy can be used to qualitatively and quantitatively assess wound healing after nerve repair. This technology, with its ability to image and subsequently quantitatively analyze intrinsic fibrillar collagen, may be a useful modality for further investigation of the variables predisposing to neuroma formation. Future studies may incorporate electrophysiology and behavioral studies in addition to SHG imaging to study different techniques for optimizing regeneration and reinnervation after nerve repair.

Samuel O. Poore, MD, PhD
Division of Plastic Surgery
Department of Surgery
University of Wisconsin School of Medicine and Public Health
600 Highland Avenue
G5/347 CSC
Madison, WI 53792
E-mail: poore@surgery.wisc.edu

ACKNOWLEDGMENT

The authors would like to thank B. Jack Longley, MD, Anatomic Pathologist and Clinical Dermatopathologist, for his contributions to this manuscript.

REFERENCES

1. Meyer RS, Abrams RA, Botte MJ, et al. Functional recovery following neurorrhaphy of the rat sciatic nerve by epineurial repair compared with tubulization. *J Orthop Res.* 1997;15:664–669.
2. Lundborg G, Rosén B. Hand function after nerve repair. *Acta Physiol (Oxf).* 2007;189:207–217.
3. Terzis JK, Sun DD, Thanos PK. Historical and basic science review: past, present, and future of nerve repair. *J Reconstr Microsurg.* 1997;13:215–225.
4. Gurtner GC, Werner S, Barrandon Y, et al. Wound repair and regeneration. *Nature.* 2008;453:314–321.
5. Koopmans G, Hasse B, Sinis N. Chapter 19: The role of collagen in peripheral nerve repair. *Int Rev Neurobiol.* 2009;87:363–379.
6. Xue M, Jackson CJ. Extracellular matrix reorganization during wound healing and its impact on abnormal scarring. *Adv Wound Care (New Rochelle).* 2015;4:119–136.
7. Vijayaraghavan S, Huq R, Hausman MR. Methods of peripheral nerve tissue preparation for second harmonic generation imaging of collagen fibers. *Methods.* 2014;66:246–255.
8. Bueno JM, Ávila FJ, Artal P. Second harmonic generation microscopy: a tool for quantitative analysis of tissues. In: Stanciu SG, ed. *Microscopy and Analysis.* InTech; 2016. Available at http://www.intechopen.com/books/microscopy-and-analysis/second-harmonic-generation-microscopy-a-tool-for-quantitative-analysis-of-tissues. Accessed May 24, 2017.
9. Gauderon R, Lukins PB, Sheppard CJ. Optimization of second-harmonic generation microscopy. *Micron.* 2001;32:691–700.
10. Chen X, Nadiarynkh O, Plotnikov S, et al. Second harmonic generation microscopy for quantitative analysis of collagen fibrillar structure. *Nat Protoc.* 2012;7:654–669.
11. Denk W, Strickler JH, Webb WW. Two-photon laser scanning fluorescence microscopy. *Science.* 1990;248:73–76.
12. Sinclair EB, Andarawis-Puri N, Ros SJ, et al. Relating applied strain to the type and severity of structural damage in the rat median nerve using second harmonic generation microscopy. *Muscle Nerve.* 2012;46:899–907.
13. Zipfel WR, Williams RM, Webb WW. Nonlinear magic: multiphoton microscopy in the biosciences. *Nat Biotechnol.* 2003;21:1369–1377.
14. Chen AC, McNeilly C, Liu AP, et al. Second harmonic generation and multiphoton microscopic detection of collagen without the need for species specific antibodies. *Burns.* 2011;37:1001–1009.
15. Cox G, Kable E, Jones A, et al. 3-dimensional imaging of collagen using second harmonic generation. *J Struct Biol.* 2003;141:53–62.
16. LeBert DC, Squirrell JM, Rindy J, et al. Matrix metalloproteinase 9 modulates collagen matrices and wound repair. *Development.* 2015;142:2136–2146.
17. Williams RM, Zipfel WR, Webb WW. Interpreting second-harmonic generation images of collagen I fibrils. *Biophys J.* 2005;88:1377–1386.
18. Liu Y, Keikhosravi A, Mehta GS. Methods for quantifying fibrillar collagen alignment. *Fibros Methods Protoc.* 2017.
19. Bredfeldt JS, Liu Y, Conklin MW, et al. Automated quantification of aligned collagen for human breast carcinoma prognosis. *J Pathol Inform.* 2014;5:28.
20. Bredfeldt JS, Liu Y, Pehlke CA, et al. Computational segmentation of collagen fibers from second-harmonic generation images of breast cancer. *J Biomed Opt.* 2014;19:16007.
21. Berens P. CircStat: a MATLAB toolbox for circular statistics. *J Stat Softw.* 2009;31:1–21.

22. Oberg AL, Mahoney DW. Linear mixed effects models. In: Ambrosius WT, ed. *Topics in Biostatistics*. Vol. 404. Totowa, NJ: Humana Press; 2007:213–234. Available at http://link.springer.com/10.1007/978-1-59745-530-5_11. Accessed May 30, 2017.
23. Noble J, Munro CA, Prasad VS, et al. Analysis of upper and lower extremity peripheral nerve injuries in a population of patients with multiple injuries. *J Trauma*. 1998;45:116–122.
24. Kemp SW, Cederna PS, Midha R. Comparative outcome measures in peripheral regeneration studies. *Exp Neurol*. 2017;287(Pt 3):348–357.
25. Kelsey JL, ed. *Upper Extremity Disorders: Frequency, Impact, and Cost*. New York: Churchill Livingstone; 1997.
26. Lundborg G. A 25-year perspective of peripheral nerve surgery: evolving neuroscientific concepts and clinical significance. *J Hand Surg*. 2000;25(3):391–414.
27. Siemionow M, Brzezicki G. Chapter 8: Current techniques and concepts in peripheral nerve repair. *Int Rev Neurobiol*. 2009;87:141–172.
28. Millesi H. Peripheral nerve surgery today: turning point or continuous development? *J Hand Surg Br*. 1990;15:281–287.
29. Wood MD, Kemp SW, Weber C, et al. Outcome measures of peripheral nerve regeneration. *Ann Anat*. 2011;193:321–333.
30. Battiston B, Papalia I, Tos P, Geuna S. Chapter 1: Peripheral nerve repair and regeneration research: a historical note. *Int Rev Neurobiol*. 2009;87:1–7. doi:10.1016/S0074-7742(09)87001–3.
31. Dahlin L, Johansson F, Lindwall C, Kanje M. Chapter 28: Future perspective in peripheral nerve reconstruction. *Int Rev Neurobiol*. 2009;87:751–758.
32. Lattouf R, Younes R, Lutomski D, et al. Picrosirius red staining: a useful tool to appraise collagen networks in normal and pathological tissues. *J Histochem Cytochem*. 2014;62:751–758.
33. Wang S, Chen X, Wu W, et al. Rapid, label-free identification of cerebellar structures using multiphoton microscopy. *J Biophotonics*. 2017. doi:10.1002/jbio.201600297 [Epub ahead of print].
34. Szulczewski JM, Inman DR, Entenberg D, et al. *In vivo* visualization of stromal macrophages via label-free FLIM-based metabolite imaging. *Sci Rep*. 2016;6:25086.
35. Park JH, Sun W, Cui M. High-resolution *in vivo* imaging of mouse brain through the intact skull. *Proc Natl Acad Sci U S A*. 2015;112:9236–9241.
36. Balu M, Lentsch G, Korta DZ, et al. *In vivo* multiphoton-microscopy of picosecond-laser-induced optical breakdown in human skin. *Lasers Surg Med*. 2017;49:555–562.
37. Balu M, Mikami H, Hou J, et al. Rapid mesoscale multiphoton microscopy of human skin. *Biomed Opt Express*. 2016;7:4375–4387.
38. Ducourthial G, Leclerc P, Mansuryan T, et al. Development of a real-time flexible multiphoton microendoscope for label-free imaging in a live animal. *Sci Rep*. 2016;5(1). doi:10.1038/srep18303.
39. Lacomb R, Nadiarnykh O, Campagnola PJ. Quantitative second harmonic generation imaging of the diseased state osteogenesis imperfecta: experiment and simulation. *Biophys J*. 2008;94:4504–4514.
40. Lin SJ, Wu R Jr, Tan HY, et al. Evaluating cutaneous photoaging by use of multiphoton fluorescence and second-harmonic generation microscopy. *Opt Lett*. 2005;30:2275–2277.
41. Lin SJ, Jee SH, Kuo CJ, et al. Discrimination of basal cell carcinoma from normal dermal stroma by quantitative multiphoton imaging. *Opt Lett*. 2006;31:2756–2758.
42. Kakkad SM, Solaiyappan M, Argani P, et al. Collagen I fiber density increases in lymph node positive breast cancers: pilot study. *J Biomed Opt*. 2012;17:116017.
43. Conklin MW, Eickhoff JC, Riching KM, et al. Aligned collagen is a prognostic signature for survival in human breast carcinoma. *Am J Pathol*. 2011;178:1221–1232.
44. Tilbury KB, Campbell KR, Eliceiri KW, et al. Stromal alterations in ovarian cancers via wavelength dependent Second Harmonic Generation microscopy and optical scattering. *BMC Cancer*. 2017;17:102.
45. Drifka CR, Loeffler AG, Mathewson K, et al. Highly aligned stromal collagen is a negative prognostic factor following pancreatic ductal adenocarcinoma resection. *Oncotarget*. 2016;7:76197–76213.
46. Keikhosravi A, Bredfeldt JS, Sagar AK, et al. Second-harmonic generation imaging of cancer. *Methods Cell Biol*. 2014;123:531–546.
47. Kwan MK, Wall EJ, Massie J, et al. Strain, stress and stretch of peripheral nerve. Rabbit experiments *in vitro* and in vivo. *Acta Orthop Scand*. 1992;63:267–272.
48. Farrar MJ, Wise FW, Fetcho JR, et al. *In vivo* imaging of myelin in the vertebrate central nervous system using third harmonic generation microscopy. *Biophys J*. 2011;100:1362–1371.
49. Zoumi A, Yeh A, Tromberg BJ. Imaging cells and extracellular matrix *in vivo* by using second-harmonic generation and two-photon excited fluorescence. *Proc Natl Acad Sci U S A*. 2002;99:11014–11019.